22 Dynamical Density-Matrix Renormalization Group

Eric Jeckelmann[1] and Holger Benthien[2]

[1] Institut für Theoretische Physik, Leibniz Universität Hannover, 30167 Hannover, Germany
[2] Physical and Theoretical Chemistry Laboratory, Oxford University, Oxford OX1 3QZ, United Kingdom

The dynamical density-matrix renormalization group (DDMRG) method is a numerical technique for calculating the zero-temperature dynamical properties in low-dimensional quantum many-body systems. For the one-dimensional Hubbard model and its extensions, DDMRG allows for accurate calculations of these properties for lattices with hundreds of sites and particles and for any excitation energy. The key idea of this approach is a variational principle for dynamical correlation functions. The variational problem can be solved with a standard density-matrix renormalization group (DMRG) method. Combined with a finite-size-scaling analysis for dynamical spectra, the DDMRG method enables us to study dynamical properties in the thermodynamic limit. An efficient calculation of momentum-dependent quantities with DMRG is achieved using open boundary conditions and quasi-momenta. These techniques are illustrated with the photoemission spectral function of the half-filled one-dimensional Hubbard model.

22.1 Introduction

Calculating the dynamical correlation functions of quantum many-body systems has been a long-standing problem of theoretical physics because many experimental techniques probe these properties. For instance, solid-state spectroscopy experiments, such as optical absorption, photoemission, or nuclear magnetic resonance, measure the dynamical correlations between an external time-dependent perturbation and the response of electrons and phonons in solids [1]. Typically, the zero-temperature dynamic response of a quantum system is given by a dynamical correlation function (with $\hbar = 1$)

$$G_X(\omega + \mathrm{i}\eta) = -\frac{1}{\pi} \left\langle \psi_0 \left| X^\dagger \frac{1}{E_0 + \omega + \mathrm{i}\eta - H} X \right| \psi_0 \right\rangle , \qquad (22.1)$$

where H is the time-independent Hamiltonian of the system, E_0 and $|\psi_0\rangle$ are its ground-state energy and wavefunction, X is the quantum operator corresponding to the physical quantity which is analyzed, and $X^\dagger$ is the Hermitian conjugate of X. A small real number $\eta > 0$ is used to shift the poles of the correlation function into the complex plane. The spectral function $G_X(\omega + \mathrm{i}\eta)$ is also the Laplace transform (up to a constant prefactor) of the zero-temperature time-dependent correlation function

E. Jeckelmann and H. Benthien: *Dynamical Density-Matrix Renormalization Group*, Lect. Notes Phys. **739**, 621–635 (2008)
DOI 10.1007/978-3-540-74686-7_22

$$G_X(t \geq 0) = \langle \psi_0 | X^\dagger(t) X(0) | \psi_0 \rangle \ , \tag{22.2}$$

where $X(t)$ is the Heisenberg representation of the operator X. In general, we are interested in the imaginary part of the correlation function for $\eta \to 0$

$$I_X(\omega + \mathrm{i}\eta) = \mathrm{Im}\, G_X(\omega + \mathrm{i}\eta) = \frac{1}{\pi} \left\langle \psi_0 \left| X^\dagger \frac{\eta}{(E_0 + \omega - H)^2 + \eta^2} X \right| \psi_0 \right\rangle \ . \tag{22.3}$$

A fundamental model for one-dimensional correlated electron systems is the Hubbard model [2] defined by the Hamiltonian

$$H = -t \sum_{j;\sigma} \left(c^\dagger_{j\sigma} c_{j+1\sigma} + c^\dagger_{j+1\sigma} c_{j\sigma} \right) + U \sum_j n_{j\uparrow} n_{j\downarrow} - \frac{U}{2} \sum_j n_j \ . \tag{22.4}$$

It describes electrons with spin $\sigma = \uparrow, \downarrow$ which can hop between neighboring sites on a lattice. Here $c^\dagger_{j\sigma}$ and $c_{j\sigma}$ are creation and annihilation operators for electrons with spin σ at site j $(= 1, \ldots, N)$, $n_{j\sigma} = c^\dagger_{j\sigma} c_{j\sigma}$ are the corresponding density operators, and $n_j = n_{j\uparrow} + n_{j\downarrow}$. The hopping integral t gives rise to a single-electron band of width $4t$. The Coulomb repulsion between electrons is mimicked by a local Hubbard interaction $U \geq 0$. The chemical potential has been chosen $\mu = U/2$ so that the number of electrons is equal to the number of sites N (half-filled band) in the grand-canonical ground state and the Fermi energy is $\varepsilon_\mathrm{F} = 0$ in the thermodynamic limit. The photoemission spectral function $A(k, \omega)$ is the imaginary part of the one-particle Green's function

$$A_\sigma(k, \omega \leq 0) = \lim_{\eta \to 0} \ I_X(-\omega + \mathrm{i}\eta) \ , \tag{22.5}$$

for the operator $X = c_{k\sigma}$ which annihilates an electron with spin σ in the Bloch state with wavevector $k \in (-\pi, \pi]$. This spectral function corresponds to the spectrum measured in angle-resolved photoemission spectroscopy experiments. We note that the spectral function of the Hubbard model is symmetric with respect to spatial reflection $A_\sigma(-k, \omega) = A_\sigma(k, \omega)$ and spin-reflection $A_\uparrow(k, \omega) = A_\downarrow(k, \omega)$. The one-particle density of states (DOS) is

$$n_\sigma(\omega \leq 0) = \frac{1}{N} \sum_k A_\sigma(k, \omega) \ . \tag{22.6}$$

At half-filling the inverse photoemission spectral function $B_\sigma(k, \omega \geq 0)$ is related to $A_\sigma(k, \omega)$ through the relation $B_\sigma(k, \omega) = A_\sigma(k + \pi, -\omega)$ and thus $n_\sigma(\omega \geq 0) = \frac{1}{N} \sum_k B_\sigma(k, \omega)$ is equal to $n_\sigma(-\omega)$.

Since its invention in 1992 the DMRG method [3, 4] has established itself has the most powerful numerical method for studying the properties of one-dimensional lattice models such as the Hubbard model (for reviews, see [5, 6, 7]). Several approaches have been developed to obtain excited states or to calculate dynamical quantities with DMRG. We will first discuss a few approaches which are both simple and efficient but do not allow for the calculation of continuous or complicated

spectra. Then we will present the dynamical DMRG method, which is presently the best frequency-space DMRG approach for calculating zero-temperature dynamical correlation functions when the spectrum is complex or continuous and allows us to determine spectral properties in the thermodynamic limit (i.e., for infinitely large lattices). The basic principles of the DMRG method are described in the Chaps. 20 and 21 of this book and are assumed to be known. The direct calculation of time-dependent quantities (22.2) within DMRG is explained in Chap. 23 while methods for computing dynamical quantities at finite temperature are described in Chap. 25.

22.2 Methods for Simple Discrete Spectra

22.2.1 Direct Evaluation of Excited States

Let $\{|n\rangle, n = 0, 1, 2, \dots\}$ be the complete set of eigenstates of H with eigenenergies E_n ($|n = 0\rangle$ corresponds to the ground state $|\psi_0\rangle$). The spectrum (22.3) can be written

$$I_X(\omega + \mathrm{i}\eta) = \frac{1}{\pi} \sum_n |\langle n|X|0\rangle|^2 \frac{\eta}{(E_n - E_0 - \omega)^2 + \eta^2} \,. \tag{22.7}$$

$E_n - E_0$ is the excitation energy and $|\langle n|X|0\rangle|^2$ the spectral weight of the n-th excited state. Obviously, only states with a finite spectral weight contribute to the dynamical correlation function. Typically, the number of contributing excited states scales as a power of the system size N (while the Hilbert space dimension increases exponentially with N). In principle, one can calculate the contributing excited states only and reconstruct the spectrum from the sum over these states (22.7).

The simplest method for computing excited states within DMRG is to target the lowest M eigenstates $|\psi_s\rangle$ instead of the sole ground state using the standard algorithm. In that case, the density matrix is formed as the sum

$$\rho = \sum_{s=1}^{M} c_s \rho_s \tag{22.8}$$

of the density matrices $\rho_s = |\psi_s\rangle\langle\psi_s|$ for each target state [8]. As a result the DMRG algorithm produces an effective Hamiltonian describing these M states accurately. Here the coefficients $c_s > 0$ are normalized weighting factors ($\sum_s c_s = 1$), which allow us to vary the influence of each target state in the formation of the density matrix. This approach yields accurate results for some problems such as the Holstein polaron [9]. In most cases, however, this approach is limited to a small number M of excited states (of the order of ten) because DMRG truncation errors grow rapidly with the number of targeted states (for a fixed number of density-matrix eigenstates kept). This is not sufficient for calculating a complete spectrum for a large system and often does not even allow for the calculation of low-energy excitations. For instance, in the strong-coupling regime $U \gg t$ of the half-filled one-dimensional

Hubbard model, the lowest excitation contributing to the photoemission spectral function $A(k,\omega)$ has an energy $-\omega = E_n - E_0 \approx U/2$ while there are many spin excitations with energies smaller than $U/2$. Therefore, in order to obtain the first contributing excitation, one would have to target an extremely large number M of eigenstates with DMRG.

22.2.2 Quantum Numbers and Symmetries

The simplest DMRG method for calculating specific excited states (rather than the lowest eigenstates) uses the conserved quantum numbers and the symmetries of the system. If quantum numbers and symmetry operators are well-defined in every subsystem, DMRG calculations can be carried out to obtain the lowest eigenstates in a specific symmetry subspace and for specific quantum numbers. As an example, the total number of particles is conserved in the Hubbard model (i.e., the particle number operator $N = \sum_j n_j$ commutes with the Hamilton operator H). Thus one can target the M lowest eigenstates for a given number of particles. This yields useful information about excitations contributing to the spectral functions $A(k,\omega)$ and $B(k,\omega)$. For instance, a gap in the density of states $n_\sigma(\omega)$ is given by

$$E_\mathrm{c} = E_0(+1) + E_0(-1) - 2E_0(0) \;, \tag{22.9}$$

where $E_0(z)$ is the lowest eigenenergy for a system with z electrons added or removed from the half-filled band.

It is also possible to target simultaneously the lowest eigenstates for two different sets of quantum numbers or in two different symmetry subspaces using (22.8) and thus to calculate matrix elements $\langle n|X|0\rangle$ between these states. This allows one to reconstruct the dynamical correlation function at low energy using the Lehmann representation (22.7). For instance, to calculate the photoemission spectral function (22.5) of the Hubbard model we would target the ground state for N electrons and the lowest M eigenstates with $N-1$ electrons as only those states contribute to $A(k,\omega)$. This way we circumvent the many low-energy spin excitations in the N-electron subspace. In practice, this method works only for the onset of the spectrum because there are still a large number of weightless spin excitations between successive $(N-1)$-electron states contributing to $A(k,\omega)$ and one would again have to target a very large number M of eigenstates to access the relevant high-energy excitations.

Using quantum numbers and symmetries is the most efficient and accurate method for calculating specific low-lying excited states with DMRG. For instance, symmetries and quantum numbers have been used successfully to study optical excitations and the low-energy optical conductivity spectrum in various extended one-dimensional Hubbard models describing conjugated polymers [10, 11]. However, this approach is obviously restricted to those problems which have relevant symmetries and quantum numbers and provides at most the lowest M eigenstates with the chosen symmetries and quantum numbers, where M is at most a few tens for realistic applications. Thus it is not appropriate for high-energy excitations and for complex or continuous spectra.

22.2.3 Lanczos-DMRG Method

The Lanczos-DMRG method [12, 13] combines DMRG with the Lanczos algorithm [14] to compute dynamical correlation functions. Starting from the states $|\phi_{-1}\rangle = 0$ and $|\phi_0\rangle = X|\psi_0\rangle$, the Lanczos algorithm recursively generates a set of so-called Lanczos vectors:

$$|\phi_{n+1}\rangle = H|\phi_n\rangle - a_n|\phi_n\rangle - b_n^2|\phi_{n-1}\rangle \ , \tag{22.10}$$

where $a_n = \langle\phi_n|H|\phi_n\rangle/\langle\phi_n|\phi_n\rangle$ and $b_{n+1}^2 = \langle\phi_{n+1}|\phi_{n+1}\rangle/\langle\phi_n|\phi_n\rangle$ for $n = 0, \ldots, L-1$. These Lanczos vectors span a Krylov subspace containing the excited states contributing to the dynamical correlation function (22.1). Calculating L Lanczos vectors gives the first $2L-1$ moments of a spectrum and up to L excited states contributing to it. The spectrum can be obtained from the continued fraction expansion

$$-\pi G_X(z-E_0) = \cfrac{\langle\psi_0|X^\dagger X|\psi_0\rangle}{z - a_0 - \cfrac{b_1^2}{z - a_1 - \cfrac{b_2^2}{z - \ldots}}} \ . \tag{22.11}$$

This procedure has proved to be efficient and reliable in the context of exact diagonalizations (see Chap. 18).

Within a DMRG calculation the Lanczos algorithm is applied to the effective superblock operators H and X and serves two purposes. Firstly, it is used to compute the full dynamical spectrum. Secondly, in addition to the ground state $|\psi_0\rangle$ some Lanczos vectors $\{|\phi_n\rangle, n = 0, \ldots, M \leq L\}$ are used as target (22.8) to construct an effective representation of the Hamiltonian which describes both ground state and excited states accurately. Be reminded that a target state does not need to be an eigenstate of the Hamiltonian but can be any quantum state which is well-defined and can be computed in every superblock during a DMRG sweep through the lattice. Unfortunately, DMRG truncation errors increase rapidly with the number M of target Lanczos vectors for a fixed number of density-matrix eigenstates kept and the method becomes numerically unstable. Therefore, only the first few Lanczos vectors (often only the first one $|\phi_0\rangle$) are included as target in most applications of Lanczos DMRG. In that case, the density-matrix renormalization does not necessarily converge to an optimal representation of H for all excited states contributing to a dynamical correlation function and the calculated spectrum is not always reliable. For instance, the shape of continuous spectra (for very large systems $N \gg 1$) can not be determined accurately with the Lanczos-DMRG method [13]. Nevertheless, Lanczos DMRG is a relatively simple and quick method for calculating dynamical properties within DMRG. In practice, it gives reliable and accurate results for simple discrete spectra made of (or dominated by) a few peaks only and it has been used successfully in several studies of low-dimensional correlated systems (see [6, 7]).

22.3 Dynamical DMRG

22.3.1 Correction Vector

The correction vector associated with the dynamical correlation function $G_X(\omega + \mathrm{i}\eta)$ is defined by [15]

$$|\psi_X(\omega + \mathrm{i}\eta)\rangle = \frac{1}{E_0 + \omega + \mathrm{i}\eta - H}|X\rangle \ , \tag{22.12}$$

where $|X\rangle = X|\psi_0\rangle$ is identical to the first Lanczos vector. If the correction vector is known, the dynamical correlation function can be calculated directly

$$G_X(\omega + \mathrm{i}\eta) = -\frac{1}{\pi}\langle X|\psi_X(\omega + \mathrm{i}\eta)\rangle \ . \tag{22.13}$$

To calculate a correction vector an inhomogeneous linear equation system

$$(E_0 + \omega + \mathrm{i}\eta - H)|\psi\rangle = |X\rangle \ , \tag{22.14}$$

has to be solved for the unknown state $|\psi\rangle$. Typically, the vector space dimension is very large and the equation system is solved with the conjugate gradient method [16] or other iterative methods [17].

The distinctive characteristic of a correction vector approach to the calculation of dynamical properties is that a specific quantum state (22.12) is constructed to compute the dynamical correlation function at each frequency ω. To obtain a complete dynamical spectrum, the procedure has to be repeated for many different frequencies. Therefore, in the context of exact diagonalizations the correction-vector approach is less efficient than the Lanczos technique (22.10) and (22.11). For DMRG calculations, however, this is a highly favorable characteristic. The dynamical correlation function can be determined for each frequency ω separately using effective representations of the system Hamiltonian H and operator X which describe a single excitation energy accurately. The approach can be extended to higher-order dynamic response functions such as third-order optical polarizabilities [18].

In practice, in a correction-vector DMRG calculation [13] two correction vectors with close frequencies ω_1 and ω_2 and finite broadening $\eta \sim \omega_2 - \omega_1 > 0$ are calculated from the effective superblock operators H and X and used as target (22.8) beside the ground state $|\psi_0\rangle$ and the first Lanczos vector $|X\rangle$. This is sufficient to obtain an accurate effective representation of the system excitations for frequencies $\omega_1 \lesssim \omega \lesssim \omega_2$. The spectrum is then calculated for this frequency interval using (22.13). The calculation is repeated for several (possibly overlapping) intervals to determine the spectral function over a large frequency range. This correction-vector DMRG method allows one to perform accurate calculations of complex or continuous spectra for all frequencies in large lattice quantum many-body systems [6, 7, 13].

22.3.2 Variational Principle

The success of the correction-vector DMRG method for calculating dynamical properties show that using specific target states for each frequency is the right approach. This idea can be further improved using a variational formulation of the problem [19]. Consider the functional

$$W_{X,\eta}(\omega,\psi) = \langle\psi|(E_0+\omega-H)^2+\eta^2|\psi\rangle + \eta\langle X|\psi\rangle + \eta\langle\psi|X\rangle \; . \tag{22.15}$$

For any $\eta \neq 0$ and a fixed frequency ω this functional has a well-defined and non-degenerate minimum $|\psi_{\min}\rangle$. This state is related to the correction vector (22.12) by

$$(H-E_0-\omega+\mathrm{i}\eta)|\psi_{\min}\rangle = \eta|\psi_X(\omega+\mathrm{i}\eta)\rangle \; . \tag{22.16}$$

The value of the minimum yields the imaginary part of the dynamical correlation function

$$W_{X,\eta}(\omega,\psi_{\min}) = -\pi\eta I_X(\omega+\mathrm{i}\eta) \; . \tag{22.17}$$

Therefore, the calculation of spectral functions can be formulated as a minimization problem.

This variational formulation is completely equivalent to the correction-vector method if we can calculate $|\psi_{\min}\rangle$ and $|\psi_X(\omega+\mathrm{i}\eta)\rangle$ exactly. However, if we can only calculate approximate states with an error of the order $\varepsilon \ll 1$, the variational formulation (22.17) gives the imaginary part $I_X(\omega+\mathrm{i}\eta)$ of the correlation function with an accuracy of the order of ε^2, while the correction-vector approach (22.13) yields results with an error of the order of ε.

22.3.3 DDMRG Algorithm

The DMRG method can be used to minimize the functional $W_{X,\eta}(\omega,\psi)$ and thus to calculate the dynamical correlation function $G_X(\omega+\mathrm{i}\eta)$. This approach is called the dynamical DMRG method. The minimization of the functional is easily integrated into the standard DMRG algorithm. At every step of a sweep through the system lattice, the following calculations are performed for the effective superblock operators H and X:

(i) The ground state vector $|\psi_0\rangle$ of H and its energy E_0 are calculated as in the standard DMRG method.
(ii) The state $|X\rangle = X|\psi_0\rangle$ is calculated.
(iii) The functional $W_{X,\eta}(\omega,\psi)$ is minimized using an iterative minimization algorithm. This yields the imaginary part $I_X(\omega+\mathrm{i}\eta)$ of the dynamical correlation function and the state $|\psi_{\min}\rangle$.
(iv) The correction vector is calculated using (22.16).
(v) The states $|\psi_0\rangle$, $|X\rangle$, and $|\psi_X(\omega+\mathrm{i}\eta)\rangle$ are used as target (22.8) of the density-matrix renormalization process.

The robust finite-system DMRG algorithm must be used to perform several sweeps through a lattice of fixed size. Sweeps are repeated until the procedure has converged to the minimum of $W_{X,\eta}(\omega,\psi)$.

To obtain the spectrum $I_X(\omega+\mathrm{i}\eta)$ over a range of frequencies, one has to repeat this calculation for several values of ω. The computational effort is thus roughly proportional to the number of frequencies. As with the correction-vector approach, one can perform a DDMRG calculation for two close frequencies ω_1 and ω_2 simultaneously, and then calculate the dynamical correlation function for frequencies ω between ω_1 and ω_2 without targeting the corresponding correction vectors. This approach can significantly reduce the computer time necessary to determine the spectrum over a frequency range but the results obtained for $\omega \neq \omega_1, \omega_2$ are less accurate than for the targeted frequencies $\omega = \omega_1$ and $\omega = \omega_2$.

22.3.4 Accuracy of DDMRG

First, it should be noted that DDMRG calculations are always performed for a finite parameter η. The spectrum $I_X(\omega+\mathrm{i}\eta)$ is equal to the convolution of the true spectrum $I_X(\omega)$ with a Lorentzian distribution of width η

$$I_X(\omega+\mathrm{i}\eta) = \int_{-\infty}^{+\infty} \mathrm{d}\omega' I_X(\omega') \frac{1}{\pi} \frac{\eta}{(\omega-\omega')^2+\eta^2} \; . \tag{22.18}$$

Therefore, DDMRG spectra are always broadened and it is sometimes necessary to perform several calculations for various η to determine $I_X(\omega)$ accurately. In most cases, however, the appropriate broadening for DDMRG calculations has merely the positive side effects of smoothing out numerical errors and hiding the discreteness of the spectrum, which is a finite-size effect (see the next section).

If a complete spectrum $I_X(\omega+\mathrm{i}\eta)$ has been obtained, it is possible to calculate the total spectral weight by integration and to compare it to ground state expectation values using sum rules. This provides an independent check of DDMRG results. For instance, the total weight of the photoemission spectral function must fulfill the relation

$$\int_{-\infty}^{0} \mathrm{d}\omega A_\sigma(k,\omega) = n_\sigma(k) \; , \tag{22.19}$$

where $n_\sigma(k) = \langle\psi_0|c^\dagger_{k\sigma}c_{k\sigma}|\psi_0\rangle$ is the ground state momentum distribution.

Numerous comparisons with exact analytical results and accurate numerical simulations have demonstrated the unprecedented accuracy and reliability of the dynamical DMRG method for calculating dynamical correlation functions in one-dimensional correlated systems [6, 9, 19, 20, 21, 22] and quantum impurity problems [23, 24, 25]. As an example, we show in Fig. 22.1 the local DOS of the half-filled one-dimensional Hubbard model calculated with DDMRG for two values of U. The local DOS is obtained by substituting $X = c_{j\sigma}$ and $X = c^\dagger_{j\sigma}$ for $c_{k\sigma}$ and $c^\dagger_{k\sigma}$ in the definition of the spectral functions $A(k,\omega)$ and $B(k,\omega)$, respectively.

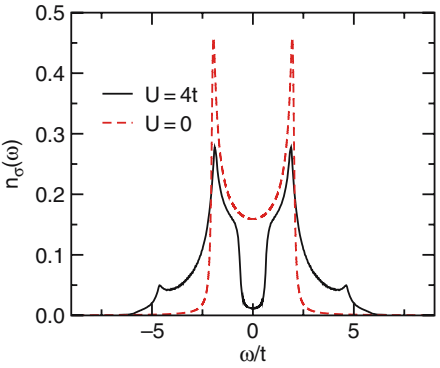

Fig. 22.1. Local density of states of the half-filled one-dimensional Hubbard model for $U = 0$ and $U = 4t$ calculated in the middle of an open chain with 128 sites using DDMRG and a broadening $\eta = 0.08t$

The local DOS does not depend on the site j for periodic boundary conditions and is equal to the integrated DOS defined in Sect. 22.1. For open boundary conditions we have checked that the local DOS in the middle of the chain is indistinguishable from the integrated DOS (22.6) for the typical broadening η used in DDMRG calculations [22]. On the scale of Fig. 22.1 the DDMRG DOS for the metallic regime ($U = 0$) is indistinguishable from the exact result (with the same broadening η), which illustrates the accuracy of DDMRG. For the insulating regime $U = 4t$, one clearly sees the opening of the Mott-Hubbard gap in Fig. 22.1. The width of the gap agrees with the exact result $E_c \approx 1.286t$ calculated with the Bethe Ansatz method [2]. The shape of the spectrum around the spectrum onsets at $\omega \approx \pm E_c/2 \approx 0.643t$ also agrees with field-theoretical predictions as discussed in the next section. The effects of the broadening $\eta = 0.08t$ are also clearly visible in Fig. 22.1: For $U = 4t$ spectral weight is seen inside the Mott-Hubbard gap and for $U = 0$ the DOS divergences at $\omega = \pm 2t$ have been broadened into two sharp peaks.

The numerical errors in the DDMRG method are dominated by the truncation of the Hilbert space. As in a ground state DMRG calculation, this truncation error decreases (and thus the accuracy of DDMRG target states and physical results increases) when more density-matrix eigenstates are kept. As the variational approach yields a smaller error in the spectrum than the correction-vector approach for the same accuracy in the targeted states, the DDMRG method is usually more accurate than the correction-vector DMRG method for the same number of density-matrix eigenstates kept or, equivalently, the DDMRG method is faster than the correction-vector DMRG method for a given accuracy.

22.4 Finite-Size Scaling

If only a finite number of eigenstates contributes to a dynamical correlation function, the spectrum (22.7) is discrete in the limit $\eta \to 0$

$$I_X(\omega) = \sum_n |\langle n|X|0\rangle|^2 \delta(E_n - E_0 - \omega) \; . \tag{22.20}$$

If the number of contributing eigenstates is infinite (for instance, in the thermodynamic limit $N \to \infty$ of the Hubbard model), the spectrum $I_X(\omega)$ may also include continuous structures. DDMRG allows us to calculate the spectrum of a large but finite system with a broadening given by the parameter η. To determine the properties of a dynamical spectrum in the thermodynamic limit, one has to calculate

$$I_X(\omega) = \lim_{\eta \to 0} \lim_{N \to \infty} I_X(\omega + \mathrm{i}\eta) \; . \tag{22.21}$$

It should be noted that the order of limits in the above formula is important. Computing both limits from numerical results requires a lot of accurate data for different values of η and N and can be the source of large extrapolation errors. A better approach is to use a broadening $\eta(N) > 0$ which decreases with increasing N and vanishes in the thermodynamic limit [19]:

$$I(\omega) = \lim_{N \to \infty} I_X(\omega + \mathrm{i}\eta(N)) \; . \tag{22.22}$$

The function $\eta(N)$ depends naturally on the specific problem studied and can also vary for each frequency ω considered. For one-dimensional correlated electron systems such as the Hubbard model, one finds empirically that the optimal scaling is

$$\eta(N) = \frac{c}{N} \; , \tag{22.23}$$

where the constant c is comparable to the effective band width of the excitations contributing to the spectrum around ω.

In Fig. 22.2 we see that the DOS of the half-filled one-dimensional Hubbard model becomes progressively step-like around $\omega \approx 0.643t$ as the system size is increased using a size-dependent broadening $\eta = 10.24t/N$. The slope of $n_\sigma(\omega)$ has a maximum at a frequency which tends to half the value of the Mott-Hubbard gap $E_\mathrm{c} \approx 1.286t$ for $N \to \infty$. The height of the maximum diverges as $\eta^{-1} \sim N$ for increasing N (see the inset in Fig. 22.2). This demonstrates the presence of a Dirac-function peak $\delta(\omega - E_\mathrm{c}/2)$ in the derivative of $n_\sigma(\omega)$ [19] or, equivalently, a step increase of the DOS at the spectrum onset in the thermodynamic limit, in agreement with the field-theoretical result for a one-dimensional Mott insulator [26]. Thus the features of the infinite-system spectrum can be determined accurately from DDMRG data for finite systems using a finite-size scaling analysis with a size-dependent broadening $\eta(N)$.

It should be noted that a good approximation for a continuous infinite-system spectrum can sometimes be obtained at a much lower computational cost than this scaling analysis by solving the convolution equation (22.18) numerically for an unknown smooth function $I_X(\omega')$ using DDMRG data for a finite system on the left-hand side (deconvolution) [9, 24, 27].

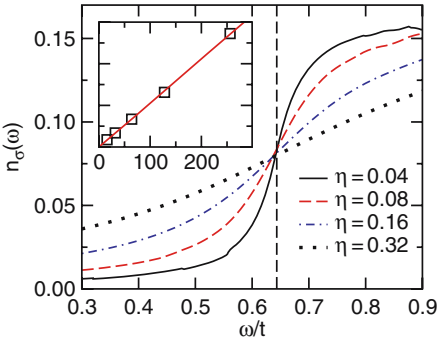

Fig. 22.2. Expanded view of the DOS around the spectrum onset at $\omega = E_c/2 \approx 0.643t$ (*vertical dashed line*) in the the half-filled one-dimensional Hubbard model for $U = 4t$. The data have been obtained with DDMRG for various system sizes from $N = 32$ to $N = 256$ with a broadening $\eta = 10.24t/N$. The inset shows the slope of $n_\sigma(\omega)$ at $\omega = E_c/2$ as a function of the system size

22.5 Momentum-Dependent Quantities

The DMRG method is usually implemented in real space where it performs optimally for one-dimensional systems with open boundary conditions and short-range interactions only [5, 6]. If periodic boundary conditions are used, momentum dependent operators, such as the operators $c_{k\sigma}$ used in the definition of the spectral functions $A(k,\omega)$, can be readily expanded as a function of local (real space) operators using plane waves (or Bloch states) [12]

$$c_{k\sigma} = \frac{1}{\sqrt{N}} \sum_{j=1}^{N} \mathrm{e}^{-\mathrm{i}kj} c_{j\sigma} \ , \tag{22.24}$$

with wavevectors $k = 2\pi z/N$ (momentum $p = \hbar k$) for integers $-N/2 < z \leq N/2$. These plane waves are the one-electron eigenstates of the Hamiltonian (22.4) in the non-interacting limit ($U = 0$) for periodic boundary conditions.

Since DMRG calculations can be performed for much larger systems using open boundary conditions, it is desirable to extend the definition of the spectral function $A(k,\omega)$ to that case. Combining plane waves with filter functions to reduce boundary effects is a possible approach [13] but this method is complicated and does not always yield good results [22]. A simple and efficient approach is based on the eigenstates of the particle-in-a-box problem [i.e., the one-electron eigenstates of the Hamiltonian (22.4) with $U = 0$ on an open chain]. The operators are defined for quasi-wavevectors $k = \pi z/(N+1)$ (quasi-momenta $p = \hbar k$) with integers $1 \leq z \leq N$ by

$$c_{k\sigma} = \sqrt{\frac{2}{N+1}} \sum_{j=1}^{N} \sin(kj) c_{j\sigma} \ . \tag{22.25}$$

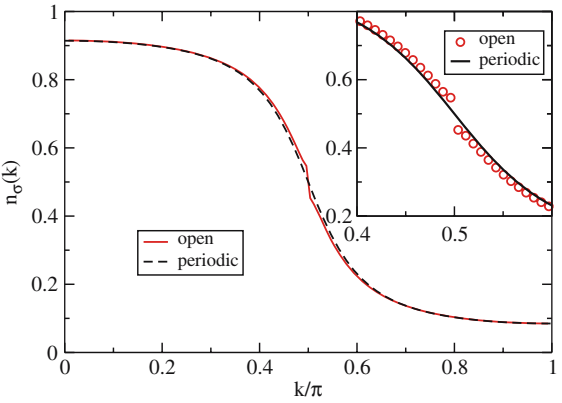

Fig. 22.3. Momentum and quasi-momentum distribution in the half-filled one-dimensional Hubbard model for $U = 4t$ calculated using DMRG on a 128-site lattice with periodic and open boundary conditions, respectively. The inset shows an expanded view of the same data around the Fermi point $k_\mathrm{F} = \pi/2$

Both definitions of $c_{k\sigma}$ are equivalent in the thermodynamic limit $N \to \infty$. Numerous test for momentum-dependent quantities [such as the spectral function $A(k, \omega)$] have shown that both approaches are also consistent in the entire Brillouin zone for finite systems [21, 22]. For instance, in Fig. 22.3 we show the ground state momentum distribution $n_\sigma(k)$ of the half-filled one-dimensional Hubbard model calculated with DMRG for both periodic and open boundary conditions. Small quantitative differences are observed only for a few special k-points corresponding to low-energy excitations, close to the Fermi wavevector $k_\mathrm{F} = \pi/2$. Therefore, open chains and the definition (22.25) can be used to investigate momentum-dependent quantities such as spectral functions $A(k, \omega)$.

22.6 Application: Spectral Function of the Hubbard Model

The DDMRG method and the quasi-momentum technique allow us to calculate the spectral properties of one-dimensional correlated systems on large lattices. To illustrate the capability of this approach we have calculated the photoemission spectral function $A_\sigma(k, \omega)$ of the half-filled one-dimensional Hubbard model. In Fig. 22.4 we show a density plot of this spectral function for $U = 4t$ on a 128-site lattice. Results for stronger coupling U/t are qualitatively similar [22]. In Fig. 22.4 we observe dispersive structures which correspond well to the excitation branches (spinon and holon) predicted by field theory for one-dimensional Mott insulators in the weak coupling regime (i.e., $U/t \ll 1$ in the Hubbard model) [26]. The DDMRG results can also be compared to those obtained with other numerical methods (see Chap. 19).

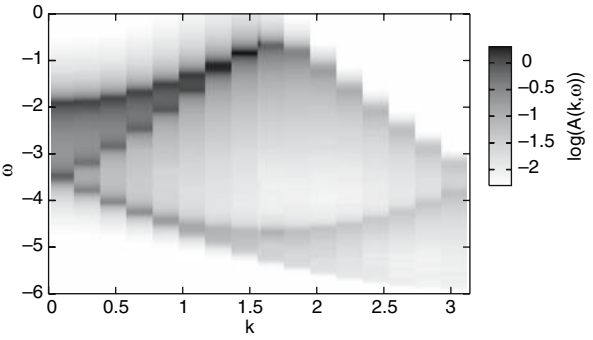

Fig. 22.4. Density plot of the spectral function $A_\sigma(k,\omega)$ in the half-filled one-dimensional Hubbard model for $U = 4t$ calculated on a 128-site open chain using DDMRG with $\eta = 0.0625t$ and quasi-momenta

An advantage of the DDMRG approach over other numerical techniques is that it allows for the simulation of systems large enough to obtain information on the spectrum in the thermodynamic limit. For instance, using the scaling analysis of Sect. 22.4 we have found that for a given k-point the spectrum maximum diverges as a power-law $\eta^{-\alpha}$ ($\sim N^{\alpha}$) for $\eta \to 0$ ($N \to \infty$) at the spectrum onset (i.e. on the low-energy holon and spinon excitation branches). This indicates a power-law divergence of the spectral weight in the thermodynamic limit [19]: $A_\sigma(k,\omega) \sim (\varepsilon(k) - \omega)^{-\alpha}$ for $\omega < \varepsilon(k)$ and $|k| \leq k_{\mathrm{F}}$, where $\varepsilon(k)$ is the gap dispersion set by the spinon branch for $|k| < Q \approx 0.4\pi$ and by the holon branch for $|k| > Q$. This behavior has been predicted for generic one-dimensional Mott insulators using field theory [26]. From the DDMRG data, we obtain $\alpha = 0.79 \pm 0.05$ for the Q-point

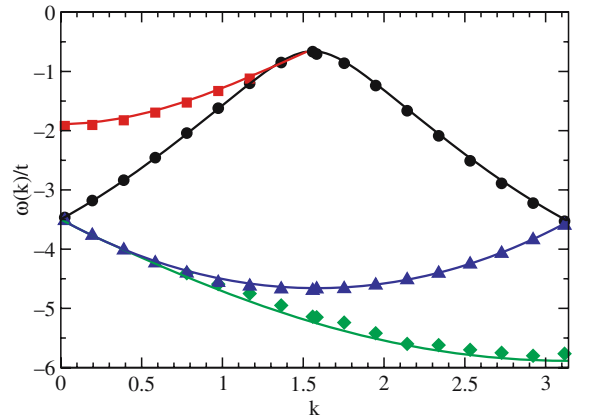

Fig. 22.5. Dispersion of structures found in the DDMRG spectral function of Fig. 22.4 (symbols). Lines show the dispersion of corresponding excitation branches calculated with the Bethe Ansatz for periodic boundary conditions

where spinon and holon branches merge and $\alpha = 0.5 \pm 0.1$ for other $|k| \leq k_{\mathrm{F}}$ in excellent agreement with the field-theoretical predictions $\alpha = 3/4$ and $\alpha = 1/2$, respectively.

Finally, we note that in the one-dimensional Hubbard model the dispersion of excitations (but not their spectral weight) can be calculated with the Bethe Ansatz method [2]. In Fig. 22.5 we compare the dispersion of structures observed in the DDMRG spectral function for an open chain with the dispersion of some excitations obtained with the Bethe Ansatz for periodic boundary conditions. The agreement is excellent and allows us to identify the dominant structures, such as the spinon branch (squares) and the holon branches (circles) [21, 22]. This demonstrates once again the accuracy of the DDMRG method combined with the quasi-momenta technique. In summary, DDMRG provides a powerful and versatile approach for investigating the dynamical properties in low-dimensional lattice quantum many-body systems.

References

1. H. Kuzmany, *Solid-State Spectroscopy* (Springer, Berlin, 1998) 621
2. F. Essler, H. Frahm, F. Göhmann, A. Klümper, V. Korepin, *The One-Dimensional Hubbard Model* (Cambridge University Press, Cambridge, 2005) 622, 629, 634
3. S.R. White, Phys. Rev. Lett. **69**(19), 2863 (1992) 622
4. S.R. White, Phys. Rev. B **48**(14), 10345 (1993) 622
5. I. Peschel, X. Wang, M. Kaulke, K. Hallberg (eds.), *Density-Matrix Renormalization, A New Numerical Method in Physics* (Springer, Berlin, 1999) 622, 631
6. U. Schollwöck, Rev. Mod. Phys. **77**(1), 259 (2005) 622, 625, 626, 628, 631
7. K. Hallberg, Adv. Phys. **55**, 477 (2006) 622, 625, 626
8. S.R. White, D.A. Huse, Phys. Rev. B **48**(6), 3844 (1993) 623
9. E. Jeckelmann, H. Fehske, in *Proceedings of the International School of Physics "Enrico Fermi" - Course CLXI Polarons in Bulk Materials and Systems with Reduced Dimensionality* (IOS Press, Amsterdam, 2006), pp. 247–284 623, 628, 630
10. S. Ramasesha, S.K. Pati, H.R. Krishnamurthy, Z. Shuai, J.L. Brédas, Phys. Rev. B **54**(11), 7598 (1996) 624
11. M. Boman, R.J. Bursill, Phys. Rev. B **57**(24), 15167 (1998) 624
12. K.A. Hallberg, Phys. Rev. B **52**(14), R9827 (1995) 625, 631
13. T.D. Kühner, S.R. White, Phys. Rev. B **60**(1), 335 (1999) 625, 626, 631
14. E.R. Gagliano, C.A. Balseiro, Phys. Rev. Lett. **59**(26), 2999 (1987) 625
15. Z.G. Soos, S. Ramasesha, J. Chem. Phys. **90**(2), 1067 (1989) 626
16. W. Press, S. Teukolsky, W. Vetterling, B. Flannery, *Numerical Recipes in C++. The Art of Scientific Computing* (Cambridge University Press, Cambridge, 2002) 626
17. S. Ramasesha, J. Comp. Chem. **11**(5), 545 (1990) 626
18. S.K. Pati, S. Ramasesha, Z. Shuai, J.L. Brédas, Phys. Rev. B **59**(23), 14827 (1999) 626
19. E. Jeckelmann, Phys. Rev. B **66**(4), 045114 (2002) 627, 628, 630, 633
20. E. Jeckelmann, F. Gebhard, F.H.L. Essler, Phys. Rev. Lett. **85**(18), 3910 (2000) 628
21. H. Benthien, F. Gebhard, E. Jeckelmann, Phys. Rev. Lett. **92**(25), 256401 (2004) 628, 632, 634
22. H. Benthien, Dynamical properties of quasi one-dimensional correlated electron systems. Ph.D. thesis, Philipps-Universität, Marburg, Germany (2005) 628, 629, 631, 632, 634

23. F. Gebhard, E. Jeckelmann, S. Mahlert, S. Nishimoto, R. Noack, Eur. Phys. J. B **36**, 491 (2003) 628
24. S. Nishimoto, E. Jeckelmann, J. Phys. Condens. Matter **16**, 613 (2004) 628, 630
25. C. Raas, G.S. Uhrig, F.B. Anders, Phys. Rev. B **69**(4), 041102 (2004) 628
26. F.H.L. Essler, A.M. Tsvelik, Phys. Rev. B **65**(11), 115117 (2002) 630, 632, 633
27. C. Raas, G. Uhrig, Eur. Phys. J. B **45**, 293 (2005) 630